ACS OMEGA

Open Access

http://pubs.acs.org/journal/acsodf

Article

Specific Detection of Uropathogenic *Escherichia coli* via Fourier Transform Infrared Spectroscopy Using an Optical Biosensor

Isabel G. Vazquez-Gutierrez, Miguel A. Reyes-López, Sara A. Ochoa, Ariadnna Cruz-Córdova, Rigoberto Hernández-Castro, Abdú Orduña-Díaz,* and Juan Xicohtencatl-Cortes*

Cite This: *ACS Omega* 2024, 9, 27528−27536

Read Online

ACCESS | Metrics & More | Article Recommendations

ABSTRACT: Urinary tract infections (UTIs) are caused mainly by uropathogenic *Escherichia coli* (UPEC), accounting for both uncomplicated (75%) and complicated (65%) UTIs. Detecting UPEC in a specific, rapid, and timely manner is essential for eradication, and optical biosensors may be useful tools for detecting UPEC. Recently, biosensors have been developed for the selective detection of antigen−antibody-specific interactions. In this study, a methodology based on the principle of an optical biosensor was developed to identify specific biomolecules, such as the PapG protein, which is located at the tip of P fimbriae and promotes the interaction of UPEC with the uroepithelium of the human kidney during a UTI. For biosensor construction, recombinant PapG protein was generated and polyclonal anti-PapG antibodies were obtained. The biosensor was fabricated in silicon supports because its surface and anchor biomolecules can be modified through its various properties. The fabrication process was carried out using self-assembled monolayers (SAMs) and an immobilized bioreceptor (anti-PapG) to detect the PapG protein. Each stage of biosensor development was evaluated by Fourier transform infrared (FTIR) spectroscopy. The infrared spectra showed bands corresponding to the C−H, C═O, and amide II bonds, revealing the presence of the PapG protein. Then, the spectra of the second derivative were obtained from 1600 to 1700 cm^{-1} to specifically determine the interactions that occur in the secondary structures between the biological recognition element (anti-PapG antibodies) and the analyte (PapG protein) complex. The analyzed secondary structure showed β-sheets and β-turns during the detection of the PapG protein. Our data suggest that the PapG protein can be detected through an optical biosensor and that the biosensor exhibited high specificity for the detection of UPEC strains. Furthermore, these studies provide initial support for the development of more specific biosensors that can be applied in the future for the detection of clinical UPEC samples associated with ITUs.

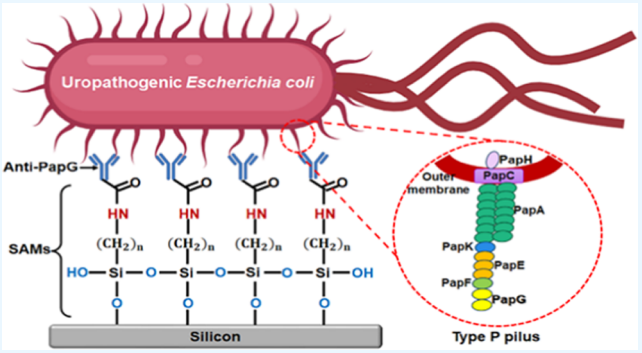

INTRODUCTION

Early and specific detection of bacterial pathogens is a primary medical goal. Globally, UPEC is a Gram-negative bacterium that causes urinary tract infections (UTIs) and is the main pathogen.[1,2]

In Mexico, UTIs are the second leading infectious disease and the third leading cause of morbidity; these infections affect women, children, elderly individuals, and immunocompromised patients.[3−5] UPEC can lose or gain genetic material by adapting to different nutritionally limited environments, evading the immune system, persisting, and spreading in the urinary tract.[3,6] UPEC can infect its host through virulence factors, which can include toxins (CNF-1, HlyA, and Sat), systems that capture iron, capsular polysaccharides, fimbrial adhesins (CsgA, DRA, FimH, FocH, PapG, and SfaS), and nonfimbrial adhesins (Tsh, Afa, and Upa).[3,7]

Type 1, type P, and curli fimbriae are found on the surface of bacterial cells and are among the most critical virulence factors that guide the first step leading to infections; these factors function by adhering to host cells, invading tissues, forming biofilms and inducing cytokine production.[8,9] FimH, a type 1 fimbrial adhesin, binds specifically to the α-D-mannose residues of membrane glycoproteins, namely, to uroplakines in the bladder epithelium,[10] and induces the formation of intracellular bacterial consortia.[3,9,11] Curli fimbriae contain large amounts of the major subunit CsgA and mediate bacterial colonization, host−pathogen interactions, host immune system evasion, and biofilm formation.[11,12]

Received: March 22, 2024
Revised: May 12, 2024
Accepted: May 24, 2024
Published: June 12, 2024

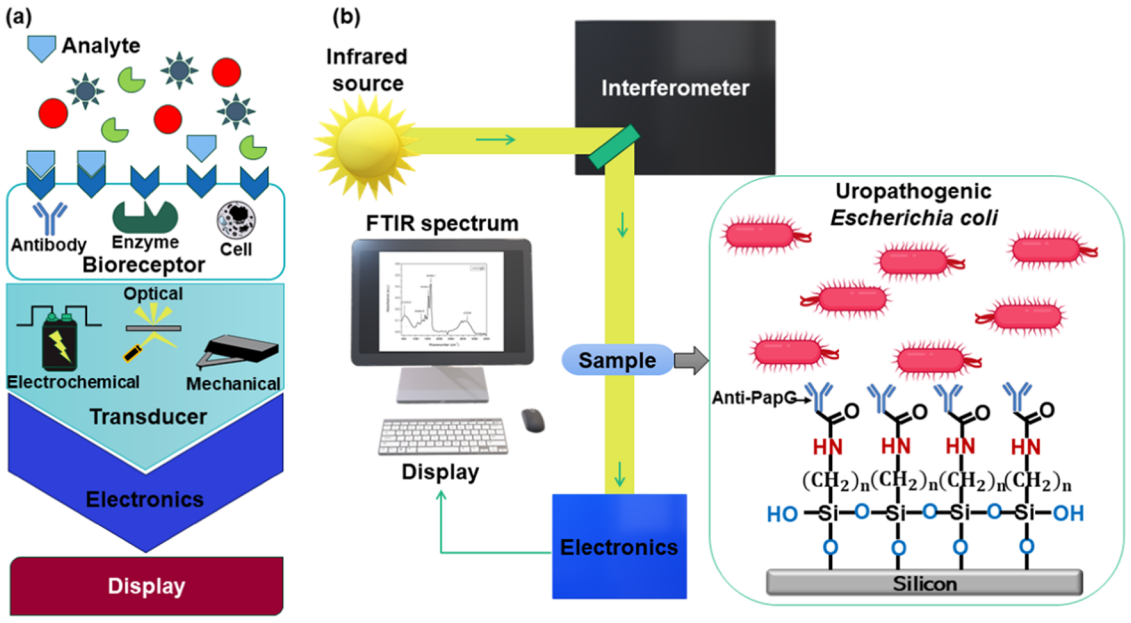

Figure 1. Schematic diagram of the biosensor. (a) Main components of typical biosensors. (b) Optical biosensor (label-free) based on the absorption of matter with infrared energy.

The protein PapG, which exhibits adhesion properties, is located on the tip of type P fimbriae and binds to glycosphingolipids; specifically, PapG binds to the Gal (α1−4β) disaccharide bond on cells in the renal epithelium, thus modulating the immune response and causing pyelonephritis.[6] Several studies have shown the assembly of these fimbriae in other bacteria; for example, type 1 fimbriae have been observed in other *Escherichia coli*, *Klebsiella* spp., *Shigella* spp., *Salmonella*, and *Citrobacter* spp., and curli fimbriae have been found in *E. coli*, *Salmonella*, *Shigella*, *Citrobacter*, and *Enterobacter* spp.[13−15] P-type fimbriae are composed of heteropolymeric fibers assembled of different protein subunits encoded by the pap A−K operon. The genes clustered in this operon are highly conserved on the chromosome of up to 90% of UPEC strains from the urinary tracts of people with acute pyelonephritis, specifically children and adults.[12,15,16] Therefore, the knowledge that the PapG protein is expressed only in UPEC strains is relevant for the specific identification of PapG using biosensors as an alternative tool for the timely detection of ITUs.

Conventional methods that are accurate and reliable, such as selective culture, biochemical, and serological methods, and automated methods, are available for the identification of *E. coli* strains.[17] These methods have certain disadvantages, as expensive biomaterials are needed; the analysis processes are complex, require several steps, and take 2−3 days; and qualified personnel are needed.[17,18] As an alternative method, biosensors are less complex, can be used to directly detect different pathogens, can achieve rapid responses, and exhibit specificity, sensitivity, and excellent versatility.[19] A typical biosensor consists of an analyte, bioreceptor or biological recognition element, transducer, electronics, and display (Figure 1a).[20−22] Analytes are substances of interest that are detected through tests, and bioreceptors are biomolecules (molecules or parts of complex molecules or supramolecular complexes) that specifically recognize analytes (e.g., enzymes, biological membranes, cell subunits, aptamers, DNA, ribonucleic acid, and antibodies).[23] The transducer is an electronic device that transforms one type of energy for biorecognition into a measurable signal. Electronics is a complex electronic circuitry that processes the transduced signal (amplifies and converts) into a measurable signal that can be displayed by a display unit. Display involves a combination of hardware and software that generates results (numeric, graphic, and tabular values or images) of the biosensor.

Biosensors can be classified as optical, mechanical, or electrochemical, depending on the transducer and response signal.[24−26] Optical biosensors consist of an optical transducer system with an integrated bioreceptor (Figure 1b). The transduction process occurs in response to physical or chemical changes generated by the interaction between the bioreceptor and analyte, including changes in light such as amplitude, absorption, phase, frequency, polarization, refraction, and transmission.[21,22,27] Optical biosensors are classified as label-free (the interaction between the bioreceptor and analyte with the transducer is detected) or label-based (the optical signal is generated by calorimetric, fluorescent, or luminescent methods).[21] The number of recognition events or detections that occur at the surface is proportional to the detected signal, which involves chemical modification and immobilization of the bioreceptor. This response involves several steps that are crucial for the fabrication of biosensors, such as the use of novel materials as substrates.[28,29] Substrates based on silicon (Si) have shown promising results in biomaterial applications (micro- and optoelectronic devices, memory chips, and sensitive biosensors) due to their semiconducting properties and biocompatibility; in addition, surface modifications and biomolecule anchoring can be easily achieved.[28] Silicon is a material that, through chemical modification of the surface through the creation of self-assembled monolayers (SAMs), can obtain interfacial properties on its surface.[30] SAMs are organized into three groups: the first is a group that binds to the surface and is known as the anchoring group; the second is a linker group that joins the anchoring group with the terminal or final group; and the latter determines the properties of the surface after SAMs treatment. The dimensions of the

https://doi.org/10.1021/acsomega.4c02794
ACS Omega 2024, 9, 27528−27536

molecular structure determine the thickness of the SAMs, which can range from 3 to 10 nm.[31,32] SAMs can be prepared using different types of molecules (e.g., silane, phosphonic acid, and thiol) and different substrates (e.g., silicon and gold).[32] The organosilane SAMs, such as 3-aminopropyltrimethoxysilane (APTMS), on Si surfaces are very stable and robust due to chemical bonding with the surface and siloxane cross-linking.[32,33] The chemical modification of the substrates begins with a cleaning process, followed by activation of the supports using piranha solution (H_2SO_4/H_2O_2) to form hydroxyl groups (−OH) on the surface of the substrate. These groups provide reactivity on the Si surfaces for greater functionalization.[34] Subsequently, functionalization occurs when APTMS contains a siloxane group and anchors the molecule to hydroxylated Si, which is connected via Si−O−Si bonds to surficial silanol groups (−SiOH).

Finally, the linking groups are composed of alkyl chains, and the terminal amino groups allow for the grafting of biologically active molecules.[28,34] For the immobilization of bioreceptors (antibodies), functionalized Si displays a terminal amine group capable of direct coupling with *N*-(3-(dimethylamino)propyl)-*N*-ethylcarbodiimide (EDC) - 1-hydroxy-2,5-pyrrolidinedione (NHS). This covalent bonding strategy involves the heterobifunctional cross-linking of the carboxyl groups of the crystallizable region of the antibodies against free amino groups on the Si surface, generating a favorable orientation of the antibodies.[28,35] Biosensors can be used to monitor target analytes, such as biomarkers, pathogens, and allergens.[36−38] Some analytes to be detected can be extracted from body fluids (saliva, sweat, blood, and urine), which are the biological components of a biosensor.[19] In this context, the objective of this study was to develop and analyze an optical biosensor as an alternative method for detecting UPEC strains in biological samples (urine) collected from pediatric patients. This biosensor, also known as an immunobiosensor, contains these antibodies as biological recognition elements to specifically interact with the PapG protein.

EXPERIMENTAL SECTION

Generation of Recombinant PapG Protein. The recombinant PapG protein was cloned, expressed, and purified based on previously established procedures with some modifications.[39] The protein was collected with a 7−1 M urea gradient via dialysis in buffer (pH 7.5) containing EDTA (0.5 mM), NaCl (100 mM), Tris (25 mM), and 3-[(3-cholamidopropyl) dimethylammonio]-1-propanesulfonate (CHAPS) (3.3 mM). The samples were incubated at 4 °C for 24 h. Protein purity and integrity were determined by polyacrylamide gel electrophoresis with 14% sodium dodecyl sulfate (SDS−PAGE). The proteins were subsequently stained with Coomassie blue, quantified according to the 2D Quant Kit protocol (GE Healthcare Biosciences AB, Björkgatan, Uppsala, Sweden), and characterized in the mid-infrared region from 400 to 4000 cm^{-1} via attenuated total reflectance (ATR) via Fourier transform infrared (FTIR) spectroscopy (Vertex 70, Bruker). The instrument had a fixed spectral resolution of 4 cm^{-1}, and the measurements were performed with a MIRacle ATR accessory and a diamond crystal sampling plate (Pike Technologies).

Generation of Rabbit Polyclonal Antibodies. Polyclonal antibodies against recombinant PapG protein were generated as described in a previously established protocol.[39] The recombinant PapG protein was detected by 14% sodium dodecyl sulfate−polyacrylamide gel electrophoresis (SDS−PAGE), visualized by Coomassie blue staining, and identified by Western blotting using anti-PapG as the primary antibody and anti-IgG as the secondary antibody. The antibody concentration was determined by the Bradford method, and the antibody structure was characterized by FTIR in ATR mode using air as a baseline. A total of 120 scans were performed with a resolution of 4 cm^{-1}. The secondary structure was determined from the second derivative of the FTIR spectrum of the antibodies.

Chemical Modification of the Silicon Surface. Commercial crystalline silicon supports (Purewafer) type P with an orientation of 100 cm, a resistivity of 5−10 Ohm*cm, and dimensions of 0.5 cm × 0.5 cm (L × L) with a thickness of 254−304 μm were used for chemical modification of the biosensors. Afterward, the samples were sonicated in 10 mL of acetone and methanol (Meyer) for 10 min each time, dried with nitrogen, and placed in a drying oven at 100 °C for 30 min. The surface was then activated by placing the samples in a solution of both sulfuric acid and hydrogen peroxide from Meyer (H_2SO_4/H_2O_2= 3:1 v/v) for 45 min. Then, the samples were washed three times with 10 mL of deionized water, dried with nitrogen, and placed in a drying oven at 100 °C for 30 min. Subsequently, the samples were immersed in an acetone solution with 5% (v/v) APTMS from Sigma-Aldrich for 45 min, sonicated in 10 mL of ethyl alcohol (Meyer) and deionized water for 10 min each, dried with nitrogen, and placed in a drying oven at 100 °C for 1 h to generate amino functional groups (NH_2) on the surface of the silicon supports. The chemical and structural compositions of the silicon supports were analyzed by FTIR in transmission mode with 120 scans at a resolution of 4 cm^{-1} within 400−4000 cm^{-1}.

Immobilization of the Bioreceptor. The antibodies were first immobilized by covalent bonding and incubated at room temperature for 15 min. Previously, a solution of anti-PapG (0.01 μg/μL) was prepared in 4-(2-hydroxyethyl)−1-piperazineethanesulfonic acid (HEPES) buffer supplemented with 8 mg/mL N-(3-(dimethylamino)propyl)-N′-ethylcarbodiimide (EDC) and 22 mg/mL *N*-hydroxysuccinimide (NHS).[40] The chemically modified supports were then incubated for 1 h at 300 rpm, washed three times with HEPES buffer, and stored at 4 °C. The immobilization of the biological recognition element was analyzed by FTIR in transmission mode with 120 scans at a resolution of 4 cm^{-1} within 400 cm^{-1} to 4000 cm^{-1}.

Detection of the Recombinant PapG Protein. The silicon supports chemically modified with the immobilized biological receptor (specific polyclonal antibodies against PapG protein) were placed in a solution with the analyte of interest (PapG protein) at a concentration of 0.01 μg/μL at 37 °C while stirring (300 rpm) for 1 h. Then, the samples were washed three times with PBS and dried under nitrogen. The results were analyzed via FTIR in transmission mode with 120 scans at a resolution of 4 cm^{-1} in the range of 4000−400 cm^{-1}. Subsequently, the secondary structures were determined from the second derivative of the spectrum.

RESULTS AND DISCUSSION

Analysis of the Recombinant PapG Protein. Coomassie blue-stained SDS−PAGE analysis revealed a protein at approximately 33.9 kDa, corresponding to the molecular weight of the recombinant PapG protein, as previously reported by our group (Figure 2a). A PapG protein concentration of 0.418 μg/μL was found, with a regression

https://doi.org/10.1021/acsomega.4c02794
ACS Omega 2024, 9, 27528−27536

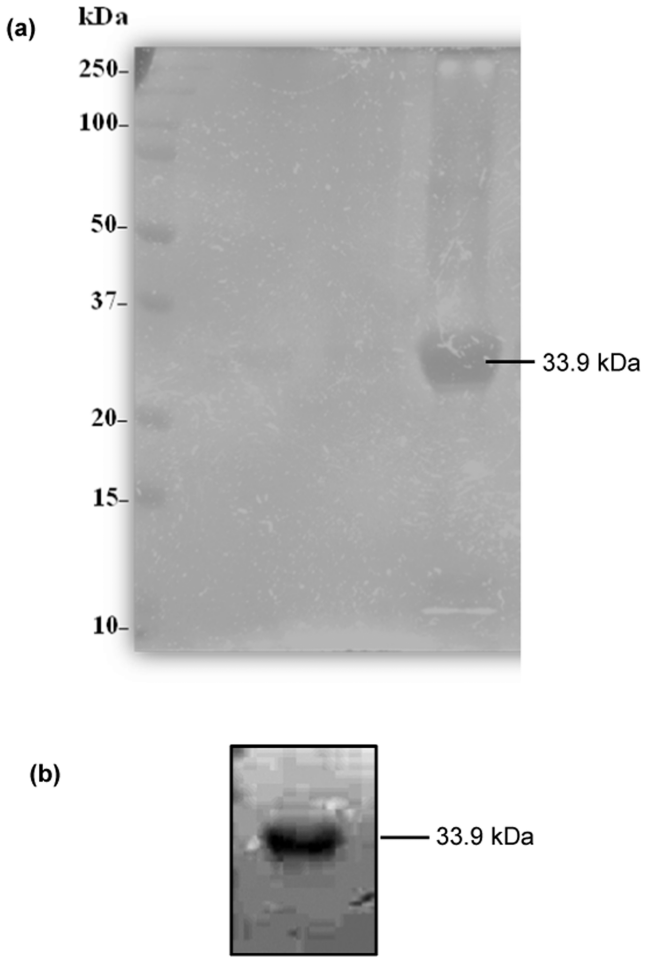

Figure 2. Identification of the recombinant PapG protein from UPEC. (a) SDS−PAGE analysis of the PapG protein. (b) Immunodetection of the PapG protein.

coefficient (R^2) of 0.979, using a standard solution of 2 mg/mL bovine serum albumin (BSA, GOLDBIO, St. Louis, MO) for the standard curve.

In the FTIR spectrum (Figure 3a), absorption bands associated with the structural composition of the PapG protein were observed. The amide VI band at 576 cm^{-1} was attributed to the bending modes in the plane of the C═O moiety,[41,42] and the amide IV band at 655 cm^{-1} was attributed to the bending vibrational modes of the O−C−N bonds (Figure 3a).[42] The band at 1048 cm^{-1} was attributed to the bending vibrational modes of the N−H bonds contributed by amide II.[43] The band at 1104 cm^{-1} was attributed to the stretching vibration of C−N and the bending vibration of the C−H bond of histidine (His) (Figure 3a).[43] The amide III band at 1237 cm^{-1} corresponded to the bending and stretching vibrational modes of N−H and C−N bonds, with a small contribution from the in-plane C−O bending vibrational modes and N−H stretching vibrational modes.[41−45] The peak attributed to COO− stretching vibrations at 1385 cm^{-1} corresponds to the amino acid side chains.[46] The band at 3266 cm^{-1} corresponding to amide A was attributed to the interaction between the vibrational modes of the N−H bond and amide II (Figure 3a).[41,43,47]

Next, deconvolution was performed in the 1500−1800 cm^{-1} region, and an amide II band at 1573 cm^{-1}, corresponding to the N−H bending vibrational modes with a contribution from the C−N stretching vibrational mode,[42,45,47,48] and an amide I band at 1625 cm^{-1}, corresponding to the stretching vibrational modes of the C═O bonds of the peptide group, were observed (Figure 3b). Notably, the amide I band was particularly sensitive to the secondary structure, and this band was mainly attributed to β-sheets in the structural conformation of the protein.[43,45,47,49,50] In addition, a band at 1795 cm^{-1} was observed, corresponding to the C═O bond stretching vibrational modes, as shown in Figure 3b.

Subsequently, the second derivative of the FTIR spectrum of the PapG protein was found in the amide I region between 1600 and 1700 cm^{-1} (Figure 3c). The following bands related to the components of the secondary structure of the protein were observed: the peaks at 1608, 1627, and 1693 cm^{-1} corresponded to β-sheets;[40,42,43,45,51] the peak at 1646 cm^{-1} corresponded to the random coil;[42,45] the peak at 1664 cm^{-1} correlated with the 3_{10} helix;[40,42] and the peak at 1676 cm^{-1} corresponded to the β-turn (Figure 3c).[42]

Characterization of Rabbit Anti-PapG Polyclonal Antibodies. Western blot analysis confirmed the identity of the PapG protein, which has a molecular weight of approximately 33.9 kDa, when specific polyclonal rabbit antibodies were used (Figure 2b). The antibody concentration was calibrated against that of BSA, which was used as a reference. The R^2 of the calibration curve was 0.98, corresponding to an antibody concentration of 2.6561 mg/mL. The FTIR spectra showed bands related to the structure of the antibodies (Figure 4a), such as the amide I band at 1643 cm^{-1}, due to the stretching vibrations of the C═O bonds of the amide group. This band was directly related to the structural conformation of the antibodies,[29,52−55] and the amide II band at 1548 cm^{-1} was attributed to in-plane N−H bending vibrations and C−N stretching vibrations (Figure 4a).[29,53,55] The amide III peak at 1243 cm^{-1} was attributed to the bending vibrational modes of N−H bonds and the stretching vibrational modes of C−N bonds (Figure 4a).[55] Analysis of the second-derivative FTIR spectra of the anti-PapG antibodies in the amide I region (1700−1600 cm^{-1}) revealed bands related to components of the secondary structure. The peak at 1631 cm^{-1} was attributed to β-sheets,[54] a band at 1650 cm^{-1} in the α-helical region,[54] and a band at 1681 cm^{-1} in the β-turn region, as shown in Figure 4b.[42]

Analysis of Silicon Substrates with Chemical Modifications. FTIR analysis of the chemical and structural compositions of the silicon supports revealed a characteristic band of silicon at 730 cm^{-1}, which corresponds to the vibration modes of the Si−O bonds (Figure 5a). Moreover, a band at 1106 cm^{-1}, corresponding to the stretching vibrational modes of the Si−O bonds (both bands generated by the interaction of oxygen coming in the environment with crystalline silicon), and a band at 612 cm^{-1}, corresponding to the stretching vibrational modes of the Si−Si bonds (Figure 5a), were observed.[29,56,57] Regarding the functional groups generated on the surface by the reaction with APTMS, characteristic bands at 1024 and 1109 cm^{-1} were attributed to the vibrational modes of the Si−O−Si bonds; these bands corresponded to the formation of siloxane bonds between the silanol groups of APTMS and were generated due to the thermal oxidation process.[56−59] Bands attributed to the C−N bending vibrational modes at 1310 cm^{-1}, C−H stretching vibrational modes at 1380 cm^{-1}, and Si−C bending vibration modes at 1445 cm^{-1} were observed, as well as a band attributed to the amino group N−H stretching vibrational mode at 1584 cm^{-1}.[29,60,61]

https://doi.org/10.1021/acsomega.4c02794
ACS Omega 2024, 9, 27528−27536

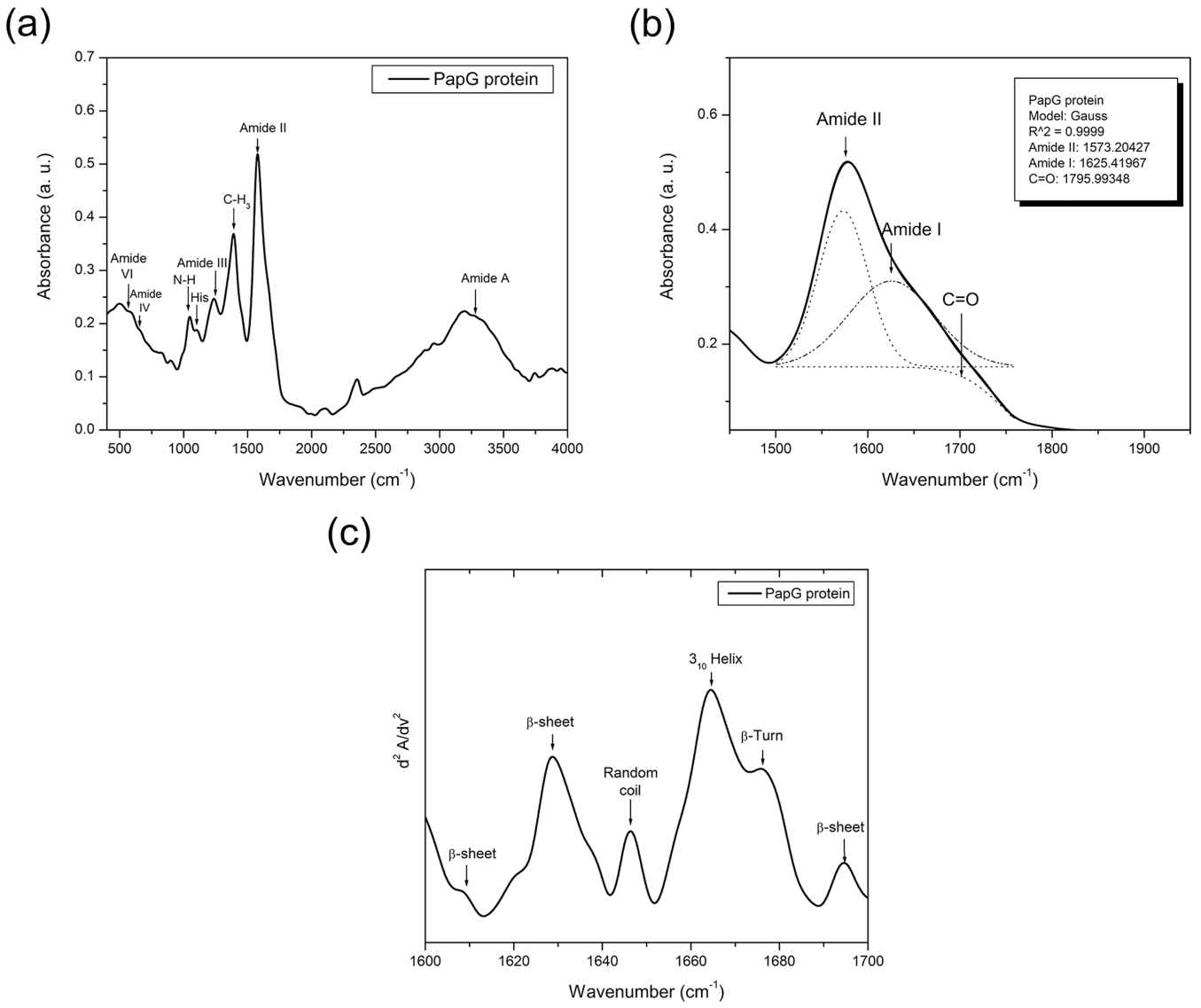

Figure 3. FTIR spectra of the recombinant PapG protein in ATR mode. (a) PapG protein. (b) Deconvolution in the region from 1400 to 1800 cm^{-1}. (c) Second derivative in the amide I region (1600−1700 cm^{-1}).

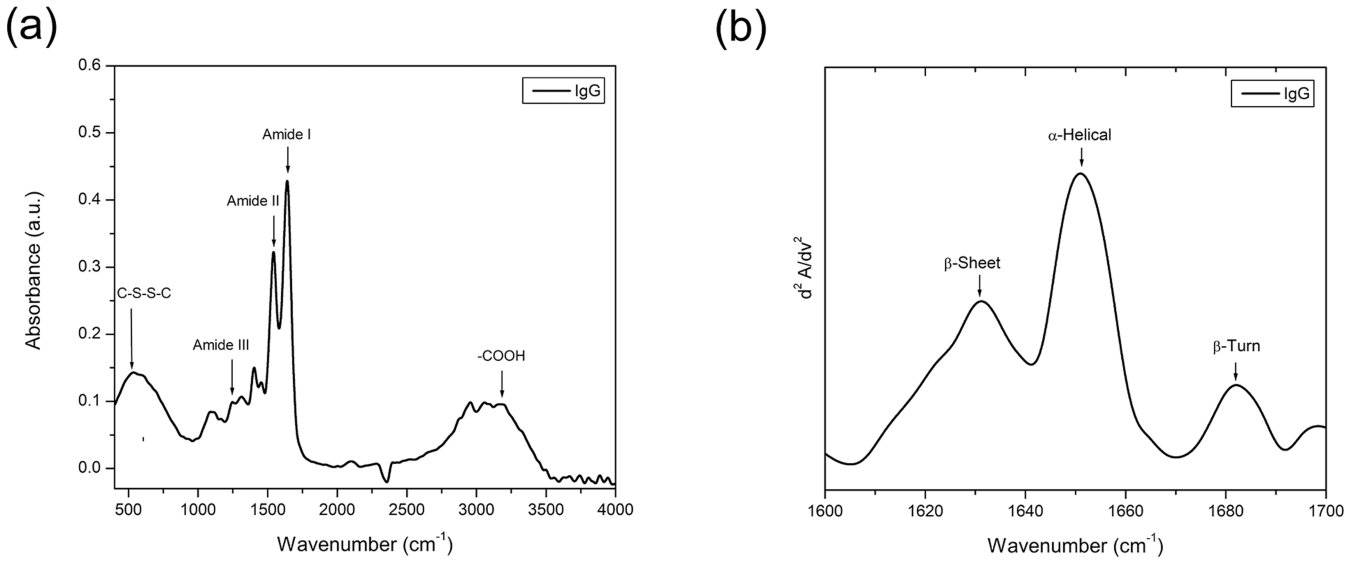

Figure 4. FTIR spectra of anti-PapG antibodies in ATR mode. (a) IgG antibodies. (b) Second derivative in the amide I region (1600−1700 cm^{-1}).

https://doi.org/10.1021/acsomega.4c02794
ACS Omega 2024, 9, 27528−27536

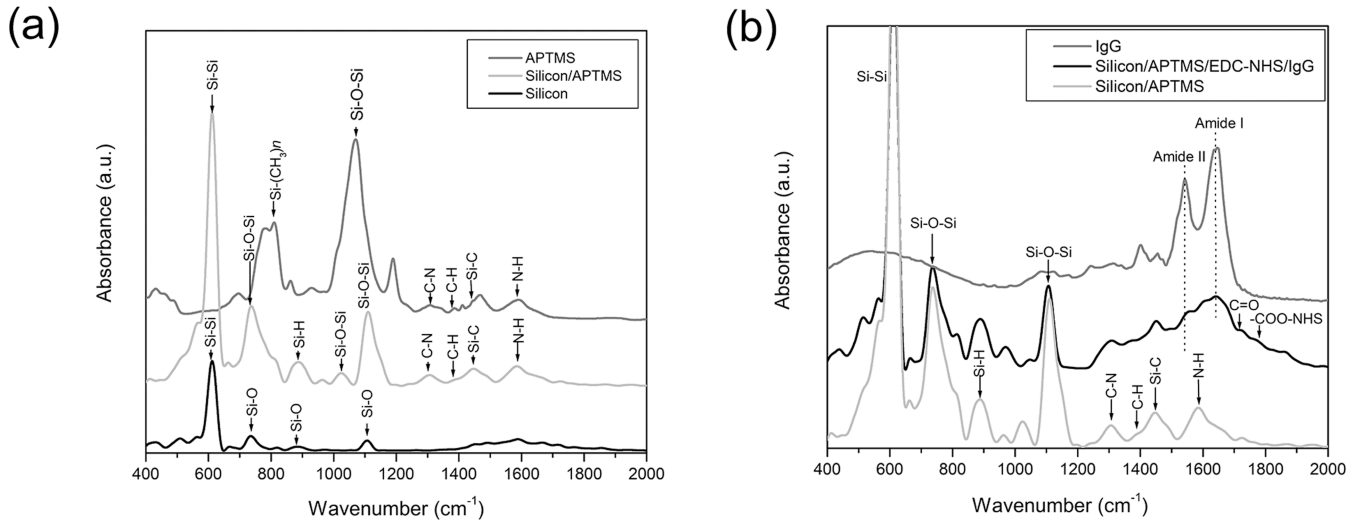

Figure 5. FTIR spectra at different stages of biosensor development. (a) Silicon sample before and after functionalization (silicon, silicon/APTMS, and pure APTMS). (b) Antibody immobilization (silicon/APTMS, silicon/APTMS/EDC-NHS/IgG, and IgG antibodies).

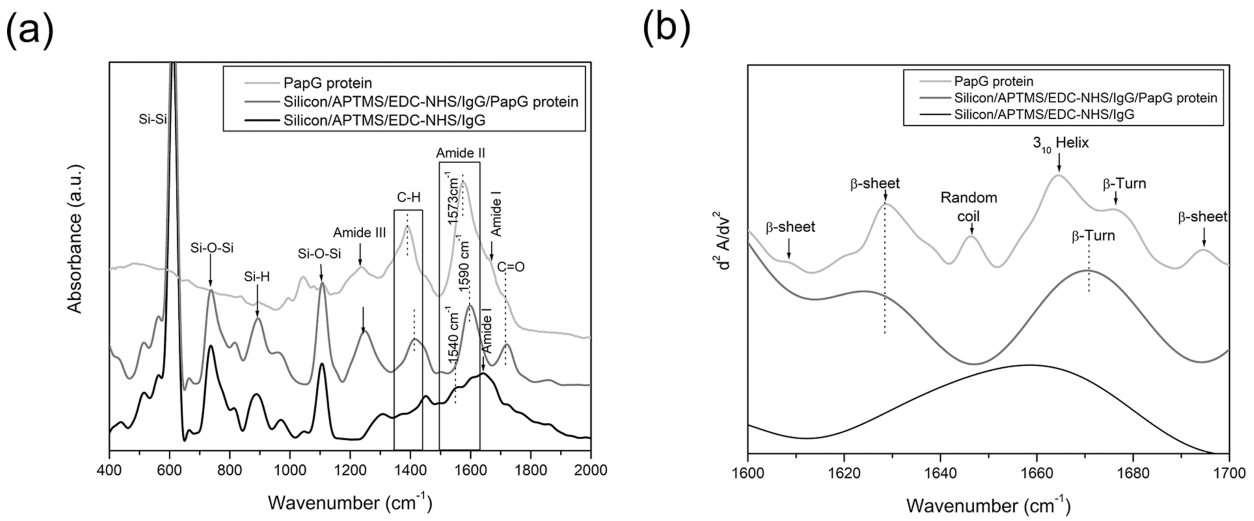

Figure 6. FTIR spectra of the samples. (a) PapG protein detection (silicon/APTMS/EDC-NHS/IgG, silicon/APTMS/EDC-NHS/IgG/PapG protein, and PapG protein). (b) Second derivative in the amide I region used to detect PapG protein (silicon/APTMS/EDC-NHS/IgG, silicon/APTMS/EDC-NHS/IgG/PapG protein, and PapG protein).

Analysis of the Immobilization of Biological Recognition Elements. The stability of bioreceptor immobilization is essential for achieving high selectivity, and noncovalent immobilization involves interactions between carboxyl/amide groups, such as electrostatic, ionic, and hydrophobic interactions, with minimal denaturation; however, these interactions can be affected by changes under physiological conditions (pH or temperature).[62,63] Covalent immobilization can eliminate this problem, but the activity of biomolecules may be compromised in some cases.[63] The immobilization of antibodies depends on the type and orientation of the antibody since these properties guarantee the availability of the paratope or Fab region for binding to the antigen. Chemical treatment with EDC-NHS is a favorable option; in this reaction, EDC binds to the carboxyl groups present in the antibodies within the fragment of the crystallizable region. Then, amide bonds are formed with the amino groups present on the surface that are chemically modified with APTMS (NHS stabilizes the intermediate in the cross-linking reaction).[40] The FTIR spectra obtained after the IgG antibodies were immobilized showed two bands corresponding to amide II and amide I associated with the immobilized antibodies. The following bands attributed to EDC/NHS were also observed: one at 1712 cm^{-1} assigned to C═O bonds and one at 1780 cm^{-1} assigned to the vibrational mode generated by the formation of a −COO-NHS ester bond, as observed in Figure 5b.[64,65]

FTIR Detection Spectral Analysis. An interaction between a specific bioreceptor and an analyte produces a measurable signal that we can detect, as contact and binding depend on adaptive stability; however, stability can be affected by several factors (pH, temperature, ionic strength, incubation time, and concentration).[29,35] After FTIR analysis was performed on the PapG protein, the spectrum showed amide II (1590 cm^{-1}), C−H (1390 cm^{-1}), and C═O (1730 cm^{-1}) bands, which were not observed during immobilization and corroborated the detection results (Figure 6a). Subsequently, to confirm the results obtained, the second derivative of the FTIR spectra was obtained in the region of the amide I protein band (1600−1700 cm^{-1}) after structural information about the IgG antibody and PapG protein complex was elucidated. In the

https://doi.org/10.1021/acsomega.4c02794
ACS Omega 2024, 9, 27528−27536

second-derivative spectra of the PapG protein, bands corresponding to the β sheets (1625 cm^{-1}) and β turns (1670 cm^{-1}) were observed (Figure 6b).[42,44] The bands observed in this analysis are not present on the supports in which the biological recognition element is immobilized and can be used for specific detection.

CONCLUSIONS

The specificities of the recombinant PapG protein and anti-PapG antibodies were validated by SDS−PAGE and Western blotting, respectively. FTIR analyses revealed bands attributed to the molecular structure of the PapG protein (C═O, amide IV, amide II, His, amide III, COO-, and amide A) and of the antibodies (amide I, amide II, and amide III). Second derivative analysis revealed differences in the molecular structure of the PapG protein (β-sheets, random coils, and 310 helices) and antibodies (β-sheets, α-helices, and β-turns).

FTIR analyses of the developed biosensor in the SAMs (Si−O−Si, C−N, C−H, Si−C, and N−H) stages, bioreceptor (amide II and amide I) immobilization, and (C−H, C═O and amide II) detection confirmed the presence of new bands in each of the stages. Our data suggest that optical biosensor development based on the interaction of energy with matter in novel substrates, such as silicon, and surface interfaces involves chemical modification by SAMs and bioreceptor immobilization for analyte-specific detection. The secondary structures (β-sheets and β-turns) detected confirmed the specificity of the PapG protein. Taken together, these data suggest that the PapG protein can be specifically detected by applying a methodology based on the principles of an optical biosensor. This study is the basis of research that provides guidelines for the continuation of the development of new experiments that allow us to validate and apply optical biosensors using clinical strains of UPEC related to ITUs.

AUTHOR INFORMATION

Corresponding Authors

Abdú Orduña-Díaz − *Centro de Investigación en Biotecnología Aplicada, Instituto Politécnico Nacional, Mexico 90700 Tlaxcala, México*; Email: aordunad@ipn.mx

Juan Xicohtencatl-Cortes − *Laboratorio de Investigación en Bacteriología Intestinal, Unidad de Enfermedades Infecciosas, Hospital Infantil de México "Federico Gómez", Mexico 06720, México*; orcid.org/0000-0003-2577-9973; Email: juanxico@yahoo.com

Authors

Isabel G. Vazquez-Gutierrez − *Centro de Investigación en Biotecnología Aplicada, Instituto Politécnico Nacional, Mexico 90700 Tlaxcala, México; Centro de Biotecnología Genómica, Instituto Politécnico Nacional, Mexico 88710 Tamaulipas, México; Laboratorio de Investigación en Bacteriología Intestinal, Unidad de Enfermedades Infecciosas, Hospital Infantil de México "Federico Gómez", Mexico 06720, México*; orcid.org/0009-0000-8941-5920

Miguel A. Reyes-López − *Centro de Biotecnología Genómica, Instituto Politécnico Nacional, Mexico 88710 Tamaulipas, México*

Sara A. Ochoa − *Laboratorio de Investigación en Bacteriología Intestinal, Unidad de Enfermedades Infecciosas, Hospital Infantil de México "Federico Gómez", Mexico 06720, México*

Ariadnna Cruz-Córdova − *Laboratorio de Investigación en Bacteriología Intestinal, Unidad de Enfermedades Infecciosas, Hospital Infantil de México "Federico Gómez", Mexico 06720, México*; orcid.org/0000-0001-8018-1275

Rigoberto Hernández-Castro − *Departamento de Ecología de Agentes Patógenos, Hospital General "Dr. Manuel Gea González", Mexico 14000, México*

Complete contact information is available at: https://pubs.acs.org/10.1021/acsomega.4c02794

Author Contributions

I.G.V.G., A.O.D., and J.X.C. designed and conceived the experiments. I.G.V.G. performed the experiments. I.G.V.G., S.A.O., M.A.R.L., A.O.D., and J.X.C analyzed the data. A.C.C., R.H.C., A.O.D., and J.X.C. contributed reagents, materials, and analysis tools. I.G.V.G., A.O.D., and J.X.C. wrote the manuscript. All authors contributed to the article and approved the submitted version.

Notes

The authors declare no competing financial interest.

ACKNOWLEDGMENTS

The authors thank the "Consejo Nacional de Humanidades, Ciencias y Tecnologías (CONAHCYT)" for awarding the scholarships with Registrations No. 637302 and No. 854926 to Isabel Gudelia Vazquez Gutierrez for the master's degree and doctorate of sciences in biotechnology at the Centro de Investigación en Biotecnología Aplicada, IPN. Grant number HIM/2018/072 SSA. 1527, HIM/2021/030 SSA. 1730, HIM/2021/031 SSA. 1720, and HIM/2022/014 SSA. 177 by Public Federal Found from the HMFG contributed to this study. In addition, the grant by the "Consejo Nacional de Humanidades, Ciencias y Tecnologías (CONAHCYT)" with grant number 319563 at the "Announcement for Basic Science and/or Frontier Science, Modality: Paradigms and Controversies of Science 2022" was an important support in the development of this study.

REFERENCES

(1) Tanabe, R. H. S.; Dias, R. C. B.; Orsi, H.; de Lira, D. R. P.; Vieira, M. A.; Dos Santos, L. F.; Ferreira, A. M.; Rall, V. L. M.; Mondelli, A. L.; Gomes, T. A. T.; Camargo, C. H.; Hern andes, R. T. Characterization of Uropathogenic *Escherichia coli* Reveals Hybrid Isolates of Uropathogenic and Diarrheagenic (UPEC/DEC) *E. coli*. *Microorganisms* **2022**, *10* (3), 645.

(2) Torres-Puig, S.; García, V.; Stærk, K.; Andersen, T. E.; Møller-Jensen, J.; Olsen, J. E.; Herrero-Fresno, A. Omics" Technologies - What Have They Told Us About Uropathogenic *Escherichia coli* Fitness and Virulence During Urinary Tract Infection? *Front. Cell. Infect. Microbiol.* **2022**, *12*, No. 824039.

(3) Ballesteros-Monrreal, M. G.; Mendez-Pfeiffer, P.; Barrios-Villa, E.; Arenas-Hernández, M. M. P.; Enciso-Martínez, Y.; Sepúlveda-Moreno, C. O.; Bolado-Martínez, E.; Valencia, D. Uropathogenic *Escherichia coli* in Mexico, an Overview of Virulence and Resistance Determinants: Systematic Review and Meta-analysis. *Arch. Med. Res.* **2023**, *54*, 247−260.

(4) Hudson, R. E.; Job, K. M.; Sayre, C. L.; Krepkova, L. V.; Sherwin, C. M.; Enioutina, E. Y. Examination of Complementary Medicine for Treating Urinary Tract Infections Among Pregnant Women and Children. *Front. Pharmacol.* **2022**, *13*, No. 883216.

(5) Kawalec, A.; Zwolińska, D. Emerging Role of Microbiome in the Prevention of Urinary Tract Infections in Children. *Int. J. Mol. Sci.* **2022**, *23* (2), 870.

(6) Flores-Mireles, A. L.; Walker, J. N.; Caparon, M.; Hultgren, S. J. Urinary tract infections: epidemiology, mechanisms of infection and treatment options. *Nat. Rev. Microbiol.* **2015**, *13* (5), 269−284.

(7) Belmont-Monroy, L.; Ribas-Aparicio, R. M.; González-Villalobos, E.; Pérez-Ramos, J. A.; Aparicio-Ozores, G.; Eslava-Campos, C. A.; Hernández-Chiñas, U.; Aquino-Andrade, A.; Balcázar, J. L.; Molina-López, J. Molecular typification of *Escherichia coli* from community-acquired urinary tract infections in Mexico. *Int. J. Antimicrob. Agents.* **2022**, *60* (4), No. 106667.
(8) Vega-Hernández, R.; Ochoa, S. A.; Valle-Rios, R.; Jaimes-Ortega, G. A.; Arellano-Galindo, J.; Aparicio-Ozores, G.; Ibarra, J. A.; Hernández-Castro, R.; Cruz-Córdova, A.; Xicohtencatl-Cortes, J. Flagella, Type I Fimbriae and Curli of Uropathogenic *Escherichia coli* Promote the Release of Proinflammatory Cytokines in a Coculture System. *Microorganisms* **2021**, *9* (11), 2233.
(9) Yang, W.; Liu, P.; Chen, Y.; Lv, Q.; Wang, Z.; Huang, W.; Jiang, H.; Zheng, Y.; Jiang, Y.; Sun, L. Dictamnine Inhibits the Adhesion to and Invasion of Uropathogenic *Escherichia coli* (UPEC) to Urothelial Cells. *Molecules.* **2022**, *27* (1), 272.
(10) Gahlot, D. K.; Taheri, N.; MacIntyre, S. Diversity in Genetic Regulation of Bacterial Fimbriae Assembled by the Chaperone Usher Pathway. *Int. J. Mol. Sci.* **2023**, *24* (1), 161.
(11) Lüthje, P.; Brauner, A. Virulence Factors of Uropathogenic *E. coli* and Their Interaction with the Host. In *Escherichia Coli - Old and New Insights*; Erjavec, M. S., Ed.; IntechOpen: Slovenia, 2023; pp 337−359 DOI: 10.5772/intechopen.99891.
(12) Shanmugasundarasamy, T.; Govindarajan, D. K.; Kandaswamy, K. A review on pilus assembly mechanisms in gram-positive and gram-negative bacteria. *Cell Surf.* **2022**, *8*, No. 100077.
(13) Desvaux, M.; Dalmasso, G.; Beyrouthy, R.; Barnich, N.; Delmas, J.; Bonnet, R. Pathogenicity Factors of Genomic Islands in Intestinal and Extraintestinal *Escherichia coli*. *Front. Microbiol.* **2020**, *11*, 2065.
(14) Klemm, P.; Schembri, M. Type 1 Fimbriae, Curli, and Antigen 43: Adhesion, Colonization, and Biofilm Formation. *EcoSal Plus* **2004**, *1* (1), No. 8.
(15) Proft, T.; Baker, E. N. Pili in gram-negative and gram-positive bacteria − structure, assembly and their role in disease. *Cell. Mol. Life Sci.* **2009**, *66* (4), 613−635.
(16) Fernández, L. A.; Berenguer, J. Secretion and assembly of regular surface structures in gram-negative bacteria. *FEMS Microbiol. Rev.* **2000**, *24* (1), 21−44.
(17) Gayathri, C. H.; Mayuri, P.; Sankaran, K.; Kumar, A. S. An electrochemical immunosensor for efficient detection of uropathogenic *E. coli* based on thionine dye immobilized chitosan/functionalized-MWCNT modified electrode. *Biosens. Bioelectron.* **2016**, *82*, 71−77.
(18) Ramesh, M.; Janani, R.; Deepa, C.; Rajeshkumar, L. Nanotechnology-Enabled Biosensors: A Review of Fundamentals, Design Principles, Materials, and Applications. *Biosensors* **2023**, *13* (1), 40.
(19) Polat, E. O.; Cetin, M. M.; Tabak, A. F.; Güven, E. B.; Uysal, B.Ö.; Arsan, T.; Kabbani, A.; Hamed, H.; Gül, S. B. Transducer Technologies for Biosensors and Their Wearable Applications. *Biosensors* **2022**, *12* (6), 385.
(20) Evtugyn, G. *Biosensors: Essentials, Lecture Notes in Chemistry 84*; Springer: Berlin, Heidelberg, 2014 DOI: 10.1007/978-3-642-40241-8.
(21) Naresh, V.; Lee, N. A Review on Biosensors and Recent Development of Nanostructured Materials-Enabled Biosensors. *Sensors* **2021**, *21* (4), 1109.
(22) Bhalla, N.; Jolly, P.; Formisano, N.; Estrela, P. Introduction to biosensors. *Essays Biochem.* **2016**, *60* (1), 1−8.
(23) Zheng, Y.; Song, X.; Fredj, Z.; Bian, S.; Sawan, M. Challenges and perspectives of multivirus biosensing techniques: A review. *Anal. Chim. Acta* **2023**, *1244*, No. 340860.
(24) Qiu, Z.; Shu, J.; Tang, D. Bioresponsive Release System for Visual Fluorescence Detection of Carcinoembryonic Antigen from Mesoporous Silica Nanocontainers Mediated Optical Color on Quantum Dot-Enzyme-Impregnated. Paper. *Anal. Chem.* **2017**, *289* (9), 5152−5160. (24)
(25) Yu, Z.; Qiu, C.; Huang, L.; Gao, Y.; Tang, D. Microelectromechanical Microsystems-Supported Photothermal Immunoassay for Point-of-Care Testing of Aflatoxin B1 in Foodstuff. *Anal. Chem.* **2023**, *2895* (8), 4212−4219. (25)
(26) Lv, S.; Zhang, K.; Zhu, L.; Tang, D.; Niessner, R.; Knopp, D. H2-Based Electrochemical Biosensor with Pd Nanowires@ZIF-67 Molecular Sieve Bilayered Sensing Interface for Immunoassay. *Anal. Chem.* **2019**, *1791* (18), 12055−12062. (26)
(27) Damborský, P.; Švitel, J.; Katrlík, J. Optical biosensors. *Essays Biochem.* **2016**, *60* (1), 91−100.
(28) Reyes-Cuellar, J. C. Immobilization of recognition elements on a self-assembled monolayers bioplatform. *DYNA* **2017**, *80* (202), 263−269.
(29) Gómez-Montaño, F. J.; Orduña-Díaz, A.; Avelino-Flores, M. C. G.; Avelino-Flores, F.; Ramos-Collazo, F.; Reyes-Betanzo, C.; López-Gayou, V. Detection of *Salmonella enterica* on silicon substrates biofunctionalized with anti-Salmonella IgG, analyzed by FTIR spectroscopy. *Rev. Mex. Ing. Quím.* **2020**, *19*, 1175−1185.
(30) Son, Y. J.; Han, J. W.; Kang, H.; Seong, S.; Han, S.; Maeda, S.; Chikami, S.; Hayashi, T.; Hara, M.; Noh, J. Formation and Thermal Stability of Ordered Self-Assembled Monolayers by the Adsorption of Amide-Containing Alkanethiols on Au(111). *Int. J. Mol. Sci.* **2023**, *24*, 3241.
(31) Kim, S.; Yoo, H. Self-Assembled Monolayers: Versatile Uses in Electronic Devices from Gate Dielectrics, Dopants, and Biosensing Linkers. *Micromachines* **2021**, *12*, 565.
(32) Ilincic, S.; Vorlaufer, G.; Franek, F.; Pauschitz, A. Surface Variation in Tribological Processes. In *Encyclopedia of Tribology*; Wang, Q. J.; Chung, Y. W., Eds.; Springer: Boston, MA, 2013 DOI: 10.1007/978-0-387-92897-5_968.
(33) Delafosse, G.; Patrone, L.; Goguenheim, D. Functionalization of silicon dioxide surface with 3-aminopropyltrimethoxysilane for fullerene C60 immobilization. *J. Nanosci. Nanotechnol.* **2011**, *11* (10), 9310−9315.
(34) Sánchez-Bodón, J.; Andrade Del Olmo, J.; Alonso, J. M.; Moreno-Benítez, I.; Vilas-Vilela, J. L.; Pérez-Álvarez, L. Bioactive Coatings on Titanium: A Review on Hydroxylation, Self-Assembled Monolayers (SAMs) and Surface Modification Strategies. *Polymers* **2022**, *14* (1), 165.
(35) Kumar, P.; Dash, S. K.; Ray, S. *Biomaterials-Based Sensors*; Springer Nature Singapore Pte Ltd: Singapore, 2023.
(36) Lu, L.; Zeng, R.; Lin, Q.; Huang, X.; Tang, D. Cation Exchange Reaction-Mediated Photothermal and Polarity-Switchable Photoelectrochemical Dual-Readout Biosensor. *Anal. Chem.* **2023**, *95* (44), 16335−16342.
(37) Zeng, R.; Qiu, M.; Wan, Q.; Huang, Z.; Liu, X.; Tang, D.; Knopp, D. Smartphone-Based Electrochemical Immunoassay for Point-of-Care Detection of SARS-CoV-2 Nucleocapsid Protein. *Anal. Chem.* **2022**, *94* (43), 15155−15161.
(38) Youxiu, L.; Qian, Z.; Dianping, T.; Reinhard, N.; Dietmar, K. Signal-On Photoelectrochemical Immunoassay for Aflatoxin B1 Based on Enzymatic Product-Etching MnO2 Nanosheets for Dissociation of Carbon Dots. *Anal. Chem.* **2017**, *89* (10), 5637−5645.
(39) Luna-Pineda, V. M.; Reyes-Grajeda, J. P.; Cruz-Córdova, A.; Saldaña-Ahuactzi, Z.; Ochoa, S. A.; Maldonado-Bernal, C.; Cázares-Domínguez, V.; Moreno-Fierros, L.; Arellano-Galindo, J.; Hernández-Castro, R.; Xicohtencatl-Cortes, J. Dimeric and Trimeric Fusion Proteins Generated with Fimbrial Adhesins of Uropathogenic *Escherichia coli*. *Front. Cell. Infect. Microbiol.* **2016**, *6*, 135.
(40) Vashist, S. K. Comparison of 1-Ethyl-3-(3-Dimethylaminopropyl) Carbodiimide Based Strategies to Crosslink Antibodies on Amine-Functionalized Platforms for Immunodiagnostic Applications. *Diagnostics* **2012**, *2* (3), 23−33.
(41) Goormaghtigh, E.; Cabiaux, V.; Ruysschaert, J. M. Determination of soluble and membrane protein structure by Fourier transform infrared spectroscopy. III. Secondary structures. *Subcell. Biochem.* **1994**, *23*, 405−450.

https://doi.org/10.1021/acsomega.4c02794
ACS Omega 2024, 9, 27528−27536

(42) Kong, J.; Yu, S. Fourier transform infrared spectroscopic analysis of protein secondary structures. *Acta Biochim. Biophys. Sin.* **2007**, *39* (8), 549−559.
(43) Barth, A. Infrared spectroscopy of proteins. *Biochim. Biophys. Acta, Bioenerg.* **2007**, *1767*, 1073−1101.
(44) Garza, G. A. B.; De La Rosa, L.; Martínez Martínez, A.; Michelb, H. C.; Cotteb, M.; Parrillaa, E. A. La microespectroscopia de infrarrojo con transformada de Fourier (FTIRM) en el estudio de sistemas biológicos. *Rev. Latinoam. Quím.* **2013**, *41*, 125−148.
(45) Haris, P. I.; Severcan, F. FTIR spectroscopic characterization of protein structure in aqueous and nonaqueous media. *J. Mol. Catal. B: Enzym.* **1999**, *7*, 207−221.
(46) Mata-Miranda, M. M.; Robles, C. I. G.; López, M. R.; Macuil, R. J. D.; Díaz, C. A. G.; Monroy, V. S.; Ishiwara, D. G. P.; Zapien, G. J. V. Principal Components by FTIR Spectroscopy as Innovative Characterization Technique during Differentiation of Pluripotent Stem Cells to Pancreatic Cells. *Rev. Mex. Ing. Bioméd.* **2017**, *38*, 225−234.
(47) Shen, X.; Wang, H.; Zhao, Y.; Liang, J.; Lu, B.; Sun, W.; Lu, K.; Wang, H.; Yuan, L. Recycling protein selective adsorption on fluorine-modified surface through fluorine-fluorine interaction. *Colloids Surf., B* **2022**, *214*, No. 112486.
(48) Di, W.; Lan, T.; Zhen, Z.; Jing, Z.; Xia, H.; Qingqing, P.; Fang, G.; Hui, L. Delivery of hyperoside by using a soybean protein isolated-soy soluble polysaccharide nanocomplex: Fabrication, characterization, and in vitrorelease properties. *Food Chem.* **2022**, *386*, No. 132837.
(49) Haris, P. I. Probing protein−protein interaction in biomembranes using Fourier transform infrared spectroscopy. *Biochim. Biophys. Acta, Biomembr.* **2013**, *1828*, 2265−2271.
(50) Jackson, M.; Mantsch, H. H. The use and misuse of FTIR spectroscopy in the determination of protein structure. *Crit. Rev. Biochem. Mol. Biol.* **1995**, *30*, 95−120.
(51) Ioannou, J. C.; Donald, A. M.; Tromp, R. H. Characterizing the secondary structure changes occurring in high density systems of BLG dissolved in aqueous pH 3 buffer. *Food Hydrocolloids* **2015**, *46*, 216−225.
(52) Boulet-Audet, M.; Kazarian, S. G.; Byrne, B. In-column ATR-FTIR spectroscopy to monitor affinity chromatography purification of monoclonal antibodies. *Sci. Rep.* **2016**, *6*, No. 30526.
(53) Byrne, B.; Beattie, J.; Song, C. L.; Sergei, G. ATR-FTIR Spectroscopy and Spectroscopic Imaging of Proteins. In *Vibrational Spectroscopy in Protein Research.*; Ozaki, Y.; Baranska, M.; Wood, B. R., Eds.; Elsevier: London, UK, 2020 DOI: 10.1016/B978-0-12-818610-7.00001-3.
(54) Schüle, S.; Frieß, W.; Bechtold-Peters, K.; Garidel, P. Conformational analysis of protein secondary structure during spray-drying of antibody/mannitol formulations. *Eur. J. Pharm. Biopharm.* **2007**, *65*, 1−9.
(55) Boulet-Audet, M.; Byrne, B.; Kazarian, S. G. High-Throughput Thermal Stability Analysis of a Monoclonal Antibody by Attenuated Total Reflection FT-IR Spectroscopic Imaging. *Anal. Chem.* **2014**, *86*, 9786−9793.
(56) Herrera-Celis, J.; Reyes-Betanzo, C.; Itzmoyotl-Toxqui, A.; Orduña-Díaz, A.; Pérez-Coyotl, A. a-SixC1−x:H thin films with subnanometer surface roughness for biological applications. *J. Vac. Sci. Technol. A* **2015**, *33*, No. 05E108.
(57) Morales-Chávez, J.; Herrera-Celis, J.; Saldana-Ahuactzi, Z.; Reyes-Betanzo, C.; Gómez-Montaño, F. J.; Orduña-Díaz, A. Silicon and hydrogenated amorphous silicon carbide as biofunctional platforms for immunosensors. *Surf. Interfaces.* **2020**, *20*, No. 100550.
(58) Soberanis-Monforte, G. A.; Gordillo-Rubio, J. L.; González-Chi, P. I. Influence of Chemically Treated Palygorskite Over the Rheological Behavior of Polypropylene Nanocomposites. *Ing. Investig. Tecnol.* **2015**, *16*, 491−501.
(59) Balderas-Valadez, R. F.; Agarwal, V. Use of porous silicon functionalized with acetylcholinesterase as detection platform for arsenic (III). *Ing. Investig. Tecnol.* **2017**, *18*, 321−329.
(60) Baranowska, M.; Slota, A. J.; Eravuchira, P. J.; Alba, M.; Formentin, P.; Pallarès, J.; Ferré-Borrull, J.; Marsal, L. F. Protein attachment to silane-functionalized porous silicon: A comparison of electrostatic and covalent attachment. *J. Colloid Interface Sci.* **2015**, *452*, 180−189.
(61) Majoul, N.; Aouida, S.; Bessaïs, B. Progress of porous silicon APTES-functionalization by FTIR investigations. *Appl. Surf. Sci.* **2015**, *331*, 388−391.
(62) Gao, S.; Guisán, J. M.; Rocha-Martin, J. Oriented immobilization of antibodies onto sensing platforms - A critical review. *Anal. Chim. Acta* **2022**, *1189*, No. 338907.
(63) Raghav, R.; Srivastava, S. Immobilization strategy for enhancing sensitivity of immunosensors: L-asparagine-AuNPs as a promising alternative of EDC-NHS activated citrate-AuNPs for antibody immobilization. *Biosens. Bioelectron.* **2016**, *78*, 396−403.
(64) Suys, O.; Derenne, A.; Goormaghtigh, E. ATR-FTIR Biosensors for Antibody Detection and Analysis. *Int. J. Mol. Sci.* **2022**, *23* (19), 11895.
(65) Widyasari, D. A.; Kristiani, A.; Randy, A.; Manurung, R. V.; Dewi, R. T.; Andreani, A. S.; Yuliarto, B.; Jenie, S. N. A. Optimized antibody immobilization on natural silica-based nanostructures for the selective detection of *E. coli*. *RSC Adv.* **2022**, *12* (33), 21582−21590.

https://doi.org/10.1021/acsomega.4c02794
ACS Omega 2024, 9, 27528−27536